Journal of Catalysis 331 (2015) 1–12

Contents lists available at ScienceDirect

Journal of Catalysis

journal homepage: www.elsevier.com/locate/jcat

Mechanistic studies of aldol condensations in UiO-66 and UiO-66-NH_2 metal organic frameworks

Julianna Hajek [a], Matthias Vandichel [a], Ben Van de Voorde [b], Bart Bueken [b], Dirk De Vos [b], Michel Waroquier [a], Veronique Van Speybroeck [a,*]

[a] Center for Molecular Modeling, Ghent University, Technologiepark 903, B-9052 Zwijnaarde, Belgium
[b] Centre for Surface Chemistry and Catalysis, University of Leuven, Kasteelpark Arenberg 23, B-3001 Leuven, Belgium

ARTICLE INFO

Article history:
Received 25 June 2015
Revised 13 August 2015
Accepted 14 August 2015

Keywords:
Aldol condensation
Jasminaldehyde
UiO-66
UiO-66-NH_2
First-principle kinetics
Heterogeneous catalysis

ABSTRACT

A full mechanistic investigation is proposed for the industrially important cross-aldol condensation reaction of heptanal with benzaldehyde on the UiO-66 and the amino-functionalized UiO-66-NH_2 metal–organic frameworks to form jasminaldehyde. Several experimental studies indicate that the activity for the aldol condensation reaction can be increased by proper functionalization of the material, e.g. by introducing an additional basic amino site and thus creating a bifunctional acid–base catalyst for the aldol condensation. The precise molecular level origin for this behavior is to date unclear. Herein state-of-the-art Density-Functional Theory (DFT) calculations have been performed to unravel the mechanism of the cross- and self-aldol condensations of benzaldehyde and propanal. To this end free energy calculations have been performed on both extended cluster and periodic models. It is found that the mechanism on both catalysts is essentially the same, although a slightly stronger adsorption of the reactants and slightly lower barriers were found on the amino functionalized material, pointing toward higher initial activities. New experiments were performed to confirm these observations. It is indeed found that the initial activity toward cross-aldol condensation on the amino functionalized material is higher, although after about 40 min of reaction both materials become equally active. Our results furthermore point out that the basic amino groups may promote side reactions such as imine formation, which is induced by water. The study as presented can assist to engineer materials at the molecular level toward the desired products.

1. Introduction

The catalytic condensation of benzaldehyde and 1-heptanal (Fig. 1) is an important aldol-type reaction in the production of α-pentyl cinnamaldehyde. This fine chemical compound of jasmine odor is commonly referred to by its commercial name jasminaldehyde and is most widely applied in the perfume industries [1].

The jasminaldehyde condensation reaction invariably goes along with the self-condensation of heptanal, leading to a major by-product, 2-pentylhept-2-enal (Fig. 1). For this reason the reaction constitutes a very interesting case to tune the selectivity of the used catalyst toward the desired product. This aldol condensation is usually carried out in the presence of a homogeneous catalyst such as sodium or potassium hydroxide [2]. The main drawbacks of the homogeneous process for the synthesis of jasminaldehyde include the absence of reusability and recycling of the catalyst, environmental pollution due to liquid alkali waste and postreaction work-up of the spent bases [3]. Apart from homogeneous catalysts, various heterogeneous catalysts such as large pore HY and beta zeolites, mesoporous aluminosilicates (Al-MCM-41), amorphous aluminophosphates (AlPO, Na-AlPO) [4], magnesium organosilicates [5], calcined hydrotalcite [3] and metal–organic frameworks [6] have been explored for the synthesis of jasminaldehyde.

Recently, metal–organic framework (MOF) compounds, which are made up of inorganic and organic moieties, have been developed into an important new class of crystalline porous materials [7–9]. Their unique structural characteristics open a range of possible application areas. MOFs have multiple uses in gas and liquid phase adsorption [10], molecular storage, drug delivery and heterogeneous catalysis [11]. Notably, a wide scope of MOF applications in catalysis is enabled by the high specific surface area and the ability to regulate their porosity by modification of both organic ligands and transition metals. The role of MOFs in the field

* Corresponding author.
E-mail address: veronique.vanspeybroeck@ugent.be (V. Van Speybroeck).

http://dx.doi.org/10.1016/j.jcat.2015.08.015
0021-9517/

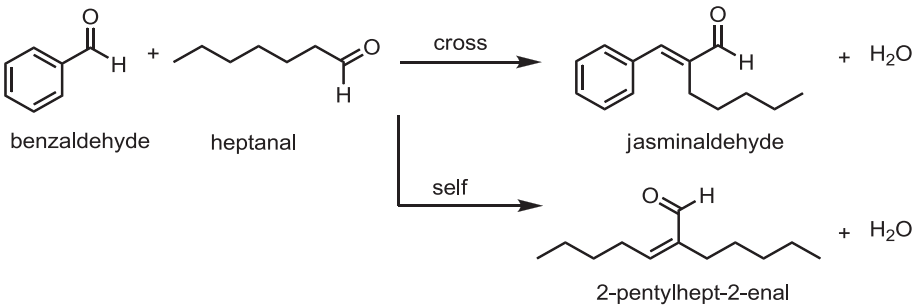

Fig. 1. Aldol condensation between benzaldehyde and heptanal (cross- and self-aldol condensations, respectively).

of catalysis has been discussed in various reviews [12–18]. One of the most widely investigated MOFs from the plethora of known frameworks is the Zr(IV)-terephthalate MOF designated as UiO-66, which has received considerable attention over the past years [19–21]. As UiO-66 possesses high thermal and chemical stability, including a good chemical resistance toward water and several alcohols, it shows promise for use in a variety of technologies [19,22]. This MOF with a cubic and rigid 3D structure consists of octahedral and tetrahedral cavities with diameters of 11 Å and 8 Å, respectively (Fig. 2). Triangular windows with a diameter of about 6 Å guarantee the access to the cages.

For Lewis acid catalyzed reactions it was shown that terephthalate defects are responsible for the catalytic activity of the UiO-66 material [23,24]. Moreover, functionalization of the 1,4-benzenedicarboxylate linker allows to obtain a family of isoreticular UiO-66 structures [23,25–28]. Such modifications to some extent affect thermal and chemical stability, and also remarkably change the electronic properties of the active site. Lescouet et al. [29] showed that the linker substitution influences the increase in catalytic activity, which arises from the enhanced Brønsted acidity. The catalytic activity of UiO-66 for several reactions was experimentally studied by different authors [23,30–35]. More specifically, the jasminaldehyde condensation has been investigated by Vermoortele et al. [6] who compared UiO-66 and UiO-66-NH_2 as catalysts for the coupling reaction between benzaldehyde and heptanal. It was proposed that UiO-66-NH_2 acts as a bifunctional catalyst with Lewis acid Zr-sites and Brønsted base –NH_2 sites, rendering it more active and selective toward jasminaldehyde [6]. Furthermore, it was proposed that the Lewis acidic $Zr_6O_4(OH)_4$ secondary building units (SBUs) activate benzaldehyde, while the amino groups on the ligand can activate the aliphatic aldehyde. The co-catalytic role of the amino groups has been assumed to partly explain the increased observed activity, but so far there has been no in depth investigation of the reaction that could support the mechanism proposed on basis of purely experimental data.

In this paper the aldol condensation is studied on the UiO-66 and UiO-66-NH_2 catalysts using first principles Density Functional Theory (DFT) calculations. The aim of this research was to find the reaction mechanism of the jasminaldehyde condensation as well as to understand the influence of the amino groups during the catalytic cycle. Furthermore new experiments have been performed on the reaction of benzaldehyde and propanal on the genuine UiO-66 and on the material modified with amino groups.

2. Methodology

2.1. Computational methods

To rationalize the reaction mechanism of the jasminaldehyde condensation, calculations were performed on an extended cluster and on a periodic model taking into account the full topology of the material, allowing an accurate quantification of the confinement effects induced by the environment of the nanoporous material. The computational methods are explained below.

An extended UiO-66 cluster was constructed following a similar procedure as used before for the MIL-47 [36] and Cu-BTC [37]

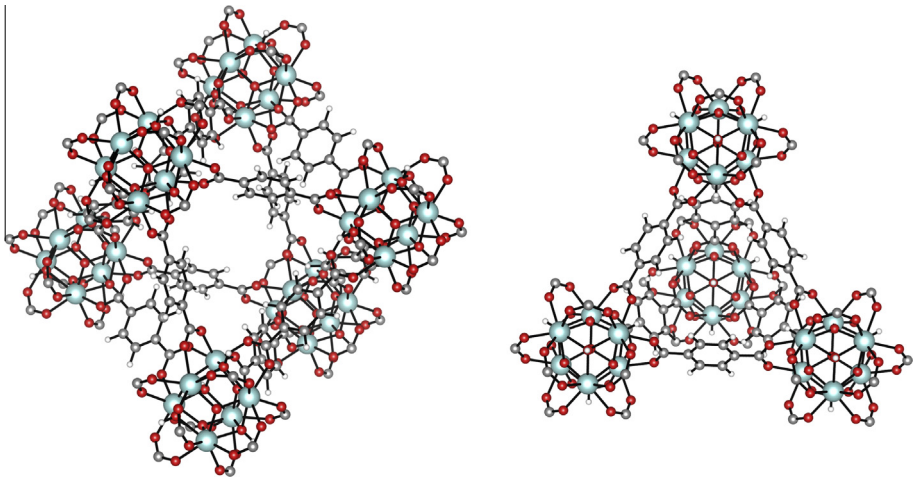

Fig. 2. Octahedral (left) and tetrahedral (right) cages of UiO-66. Color scheme: Zr (cyan); O (red); C (gray); H (white). (For interpretation of the references to color in this figure legend, the reader is referred to the web version of this article.)

metal–organic frameworks. From an optimized supercell with four inorganic groups with one terephthalate defect (unit cell formula: $[Zr_6O_5(OH)_3(RCOO)_{11}]_2[Zr_6O_4(OH)_4(RCOO)_{12}]_2$, Fig. S2) we cut an extended cluster model using the in-house developed program Zeobuilder [38]. In the cluster model seven linkers were replaced by formic group while the remaining four linkers surround the active site (Fig. 3a). The resulting two active Zr-sites have a coordination number of seven. Analogously, UiO-66-NH_2 was constructed arbitrarily by replacing a hydrogen atom by an amino group on each phenyl ring. An alternating substitution of the amino group in the *meta*- and *ortho*-position (Fig. 3b) was chosen in a similar fashion as in earlier reports [23,39]. The extended cluster calculations were performed with the Gaussian 09 package [40]. We applied the B3LYP/6-31G(d) level of theory for the geometry optimization. The energies were refined using a triple-zeta Pople basis set with one diffuse and one polarization function on each atom (level of theory: B3LYP/6-311++G(d,p)). Note that for Zr we did not use the aforementioned basis sets; instead we used the LANL2DZ basis set and pseudopotential for the geometry optimizations and LANL2TZ for the energy refinements [41–43]. We also looked at the effect of single *f* polarization function on Zr atom. However, this has a minor influence on the free energy of the reaction path. Using the standard notation "LOT-E"//"LOT-G" (LOT-E and LOT-G being the electronic levels of theory used for the energy and geometry optimizations, respectively), all cluster results discussed in this paper are obtained with the method denoted as "B3LYP/6-311++g(d,p)-D3//B3LYP/6-31g(d)*". The asterisk * points to the LANL2TZ and LANL2DZ basis set and ECP for Zr, used for

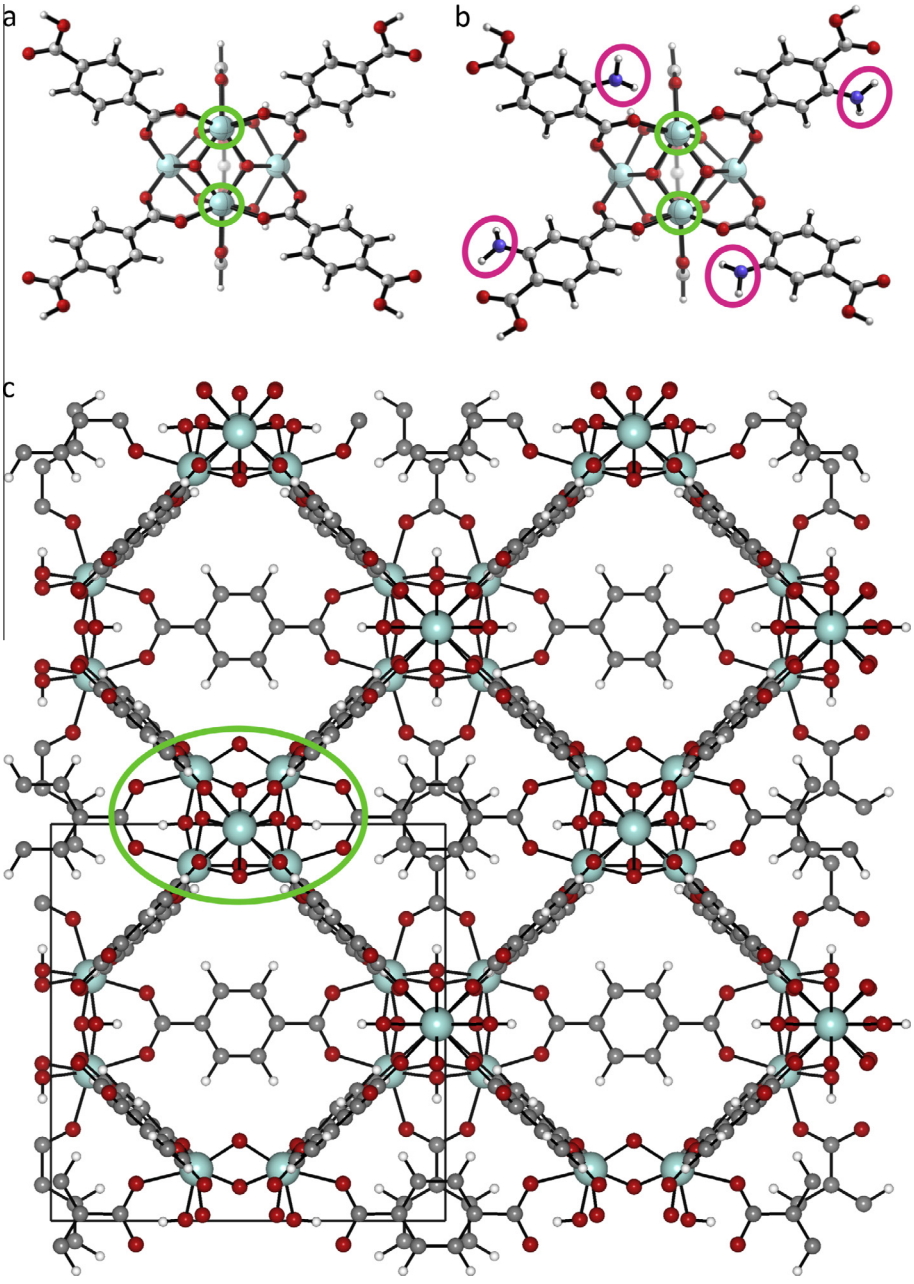

Fig. 3. Model for (a) the extended UiO-66 and (b) UiO-66-NH_2 cluster with four surrounding linkers, (c) the periodic model with the encircled active site, using the same color scheme as employed in Fig. 2. The Lewis acid sites on the cluster models are marked in green circles while amine Brønsted base sites are indicated in pink circles. (For interpretation of the references to color in this figure legend, the reader is referred to the web version of this article.)

energy refinement and geometry optimization, respectively. To account for dispersion effects, Grimme corrections of the type D3 were added to the energies, using the DFT-D3 program [44].

In contrast to cluster calculations in which only a fragment of the crystallographic structure is considered, periodic calculations take into account the entire unit cell. We construct the supercell starting from an orthorhombic unit cell. Then one linker is cut out and the geometry of the new structure is optimized with the periodic code. The active site lies in the middle of the UiO-66 unit cell (Fig. 3c). The periodic DFT-D3(BJ) calculations were performed with the Vienna Ab Initio Simulation Package (VASP 5.3) [45–48] and include dispersion effects using a damping function proposed by Becke and Johnson as implemented by Grimme [49]. The position of the active site gives only minimal interactions with neighboring unit cells. For the simulations, the Brillouin zone was sampled by the Γ-point, as the UiO-66 materials have the face-centered symmetry of the F$m-3m$ space group. To check the influence of the chosen k-point mesh, we applied a larger Brillouin zone of $2 \times 2 \times 2$ k-points and found an electronic energy that barely differed from the Γ-point (less than 0.2 kJ/mol). All structures were first optimized with a PBE-D3(BJ) exchange correlation functional and the projector augmented approximation (PAW) [50,51] together with a plane wave kinetic energy cutoff of 400 eV. The convergence criterion for the electronic self-consistent field (SCF) problem was set to 10^{-8} eV. Afterward, the energy in the periodic code was refined with the hybrid functional B3LYP-D3(BJ). For the first step of the cross-aldol condensation reaction (vide infra) we compared enthalpy, entropy and free energy contributions on both cluster and periodic models obtained with the PBE and B3LYP functional of a combination of them, as reported in Table S1 of the SI. From the reported values it is clear that the entropy contributions are hardly affected by the level of theory. In view of the computational expense of the B3LYP for geometry optimization with periodic codes we opted to use the PBE functional for the geometry optimization and to refine the energies with the B3LYP functional.

Modeling reactions with molecules containing long alkyl chains such as heptanal would be very difficult because of the multitude of possible conformations and adsorption states. This would require a first principles molecular dynamics approach [52]. Therefore, instead of heptanal we modeled the aldol condensation using propanal. The thermal corrections were performed on the basis of frequencies obtained with a partial Hessian on the systems displayed in Fig. 4 (two Zr, two bridging O and the reacting molecules, benzaldehyde and propanal or two propanal molecules). De Moor et al. [53] demonstrated that this type of procedure of using a partial Hessian is sufficient to determine accurate enthalpy and entropy differences. The obtained energy and entropy differences are similar to the ones obtained with full Hessian calculations. The nature of the transition states and local minima was verified by a normal mode analysis. In the case of a local minimum on the potential energy surface, the partial Hessian matrix has only positive eigenmodes. In the case of a transition state, there is also one imaginary eigenmode corresponding to the vibration. For both cluster and periodic models we applied the partial Hessian vibrational analysis (PHVA) [54–56] as implemented in an in-house post-processing toolkit TAMkin [57]. We used this program to investigate the enthalpic and entropic contributions to the free energy barriers.

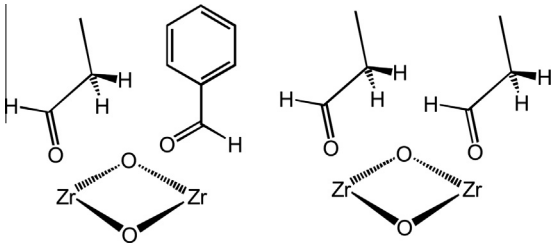

Fig. 4. Selected atoms used to compute a subsequent partial Hessian for the cross (right)- and self (left)-aldol condensations.

2.2. Experimental methodology

To facilitate the comparison between experimental findings and the new theoretical results new experiments were performed using similar reactants – benzaldehyde and propanal – as in the theoretical model, thus resulting in α-methylcinnamaldehyde formation. All chemicals were obtained commercially from Sigma Aldrich or ABCR and were used as received.

The synthesis of the materials was as follows: 13.5 mmol of terephthalic acid or 2-aminoterephthalic acid, 8.91 mmol $ZrCl_4$ and 400 ml DMF were mixed in a 1 l Schott bottle and heated up to 140 °C for 12 h. The powders were subsequently washed with 2 × DMF and 2 × ethanol. The samples were pretreated at 160 °C overnight before reaction to remove physisorbed water from the pores.

For the condensation reaction, a mixture of 0.17 mol (18.2 g) benzaldehyde (99%), 11 mmol (0.64 g) propanal (99%) and 7.7 mmol (1 g) nonane (99%) as an internal standard was used to prepare a stock solution and 1.4 ml of the solution was injected in a vial containing 150 mg (approx. 0.09 mmol) catalyst. The reaction mixture was stirred at 700 rpm and heated in an aluminum heating block at 393 K. Reaction samples were filtered through a 0.45 μm filter and analyzed with a Shimadzu 2014 GC equipped with a FID detector and an apolar CP-Sil 5 CB column. The identity of the reaction products was verified by GC–MS (Agilent 6890 gas chromatograph, equipped with a HP-5MS column, coupled to a 5973 MSD mass spectrometer).

3. Results and discussion

3.1. Reaction mechanism of the cross-aldol condensation on UiO-66

It is commonly known that the jasminaldehyde condensation occurs in the presence of a catalyst [1–6]. For the condensation of jasminaldehyde on UiO-66 as catalyst, we propose a mechanism that includes 6 steps (Fig. 5a). The mechanism relies on the availability of catalytically active sites in the UiO-66 material. In a previous work of some of the present authors, it was shown that open metal defect sites are required to make the material catalytically active. It was indeed shown that such sites arise during the synthesis of these materials [22,24,58]. These coordinatively unsaturated sites have a Lewis acid character.

We first explore the various steps of the cross-aldol reaction shown in Fig. 5a. In the proposed mechanism, both reactants are adsorbed by their carbonyl oxygen on adjacent Zr atoms (State 1-c). The free energy of adsorption of the pre-reactive complex is −45.7 kJ/mol. The 1-propanal molecule is exclusively activated by deprotonation of the α-carbon atom on the μ_3-oxygen belonging to the inorganic part of the framework (TS1). This leads to the formation of an enolate intermediate which is stabilized through interaction with the Zr active site (State 2-c). Benzaldehyde is very susceptible to attack by the Zr-bound 1-propene-1-oxide. In the beginning of step 2 (C–C coupling) Zr-bound 1-propene-1-oxide rotates and a new intermediate state is formed with an adsorption free energy of −65.8 kJ/mol. The carbon–carbon coupling reaction is exergonic and proceeds very fast with a free energy barrier of 32.9 kJ/mol (TS2). The C–C coupling product has a free energy level of −83.9 kJ/mol and is the most stable intermediate during the whole reaction path (State 3-c). In the next step

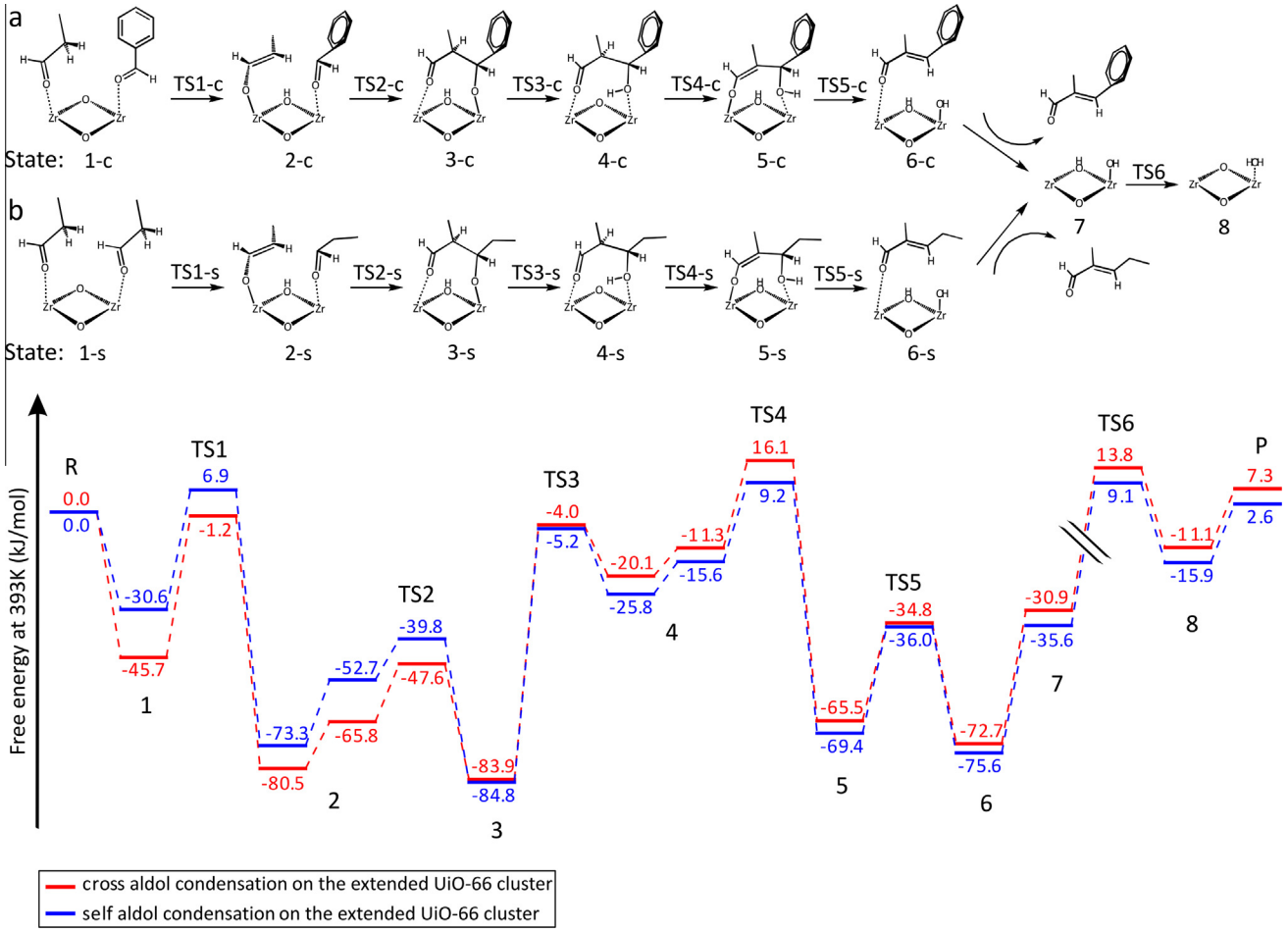

Fig. 5. Comparison of the free energy profiles (B3LYP/6-311++G(d,p)-D3//B3LYP/6-31G(d)*) of cross (red line)- and self (blue line)-aldol condensation on UiO-66, calculated at 393 K. R corresponds to the reactants in gas phase and the cluster, P corresponds to the final product and water in gas phase and the cluster. (a) Schematic representation of the cross- aldol and (b) self-aldol condensation. Two parallel bars indicate that the main product is no longer present in the catalyst. (For interpretation of the references to color in this figure legend, the reader is referred to the web version of this article.)

(step 3), the C–C coupling product gets protonated by the hydrogen attached to the μ_3-oxygen atom and this leads to the aldol product formation (State 4-c), with a free energy barrier of 79.9 kJ/mol (TS3). This free energy barrier originates from a high enthalpy ($\Delta H^{\ddagger}$ = 79.9 kJ/mol) and a nearly negligible entropy contribution. Afterward, the molecule rotates to be in an optimal position for the deprotonation of the α-carbon atom and forms the intermediate with a free energy of −11.3 kJ/mol. The μ_3-oxygen atom which belongs to the Zr-cluster is again protonated by the α-carbon atom (State 5-c). The consecutive protonation/deprotonation of the reacting molecules requires in total 100 kJ/mol to overcome the global free energy barrier on the potential energy surface (steps 3–5) and is obviously the rate determining step in the whole reaction pathway. Next, the dehydroxylation takes place by chemisorption of the hydroxyl group on the Zr Lewis acid site. The hydroxyl group is split off and the main product, in our case α-methyl-*trans*-cinnamaldehyde is formed (State 6-c). To release the product from the catalyst we need to overcome the free energy barrier of 41.8 kJ/mol (State 7). In the scheme of Fig. 5 we also include the removal of water (TS6), as water is produced during aldol condensation reactions while the α-methyl-*trans*-cinnamaldehyde stays in the gas phase. At the end of the route the catalytic cycle is closed with the catalyst, water and the main product in gas phase (State P, Fig. 5).

We also investigated a pathway in which benzaldehyde is activated on the hydroxyl group belonging to the inorganic framework but found higher free energy barriers, and thus this option was no longer retained as plausible route in the remainder of this paper.

Concluding, the lowest rate-determining free energy barrier of all possible reaction routes for the cross-aldol condensation between benzaldehyde and propanal is 100 kJ/mol (from State-3 and TS4 in Fig. 5). This barrier can probably be lowered by taking solvation effects into consideration. Explicit water molecules can assist in the proton jump from the oxo-atom to the former aldehyde oxygen. However, the study of solvation effect is out of the scope of this paper.

A similar cycle can be constructed for the formation of the major by-product 2-pentylhept-2-enal from two propanal molecules. For the self-condensation a similar reaction is proposed (Fig. 5b). The initial step is the adsorption of two propanal molecules on adjacent Zr acid sites (State 1-s). Benzaldehyde (State 1-c) is more strongly adsorbed than propanal (State 1-s), with free energies of adsorption of −45.7 and −30.6 kJ/mol, respectively. The self-aldol condensation is competitive and seems thermodynamically favored over the cross-aldol condensation. The free energy profiles for the cross- and self-aldol condensations on UiO-66 are compared in Fig. 5 which shows the Gibbs free activation barriers at 393 K. The theoretical results are given in Table 1, in which the enthalpy and entropy contributions are listed separately. Propanal, being an aliphatic aldehyde is more reactive than benzaldehyde. Consequently, the self-condensation of propanal is a parallel reaction which reduces the yield to jasminaldehyde. For

Table 1
Enthalpy, entropy and free energy contributions given in kJ/mol on the cluster model UiO-66 (B3LYP/6-311++G(d,p)-D3//B3LYP/6-31G(d)*), calculated at 393 K.

		Cross			Self		
		$\Delta H^{\ddagger}$	$-T\Delta S^{\ddagger}$	$\Delta G^{\ddagger}$	$\Delta H^{\ddagger}$	$-T\Delta S^{\ddagger}$	$\Delta G^{\ddagger}$
Cluster model UiO-66	Step 1	25.8	18.6	44.4	18.9	18.6	37.5
	Step 2	14.3	18.6	32.9	16.6	16.9	33.5
	Step 3	79.9	0.0	79.9	78.6	1.0	79.6
	Step 4	25.7	10.5	36.2	21.6	13.3	34.9
	Step 5	33.1	−2.4	30.7	40.3	−6.9	33.4
	Steps 3–5	97.0	3.0	100.0	87.5	6.5	94.0

the cross as well as the self-aldol condensations the highest entropic contribution ($-T\Delta S^{\ddagger}$ = 18.7 and 18.6 kJ/mol, respectively) is shown in step 1 whereas the lowest enthalpic contribution ($\Delta H^{\ddagger}$ = 14.3 and 16.6 kJ/mol, respectively) is observed in step 2. After the second step, a stable intermediate with sp^3 hybridization and free energy of −84.8 kJ/mol is formed (State 3-s). For both condensation reactions the free energy barrier for the protonation of the C–C coupled complex (TS3) amounts to 80.0 kJ/mol, which is very high and completely dominated by the enthalpic contribution ($\Delta H^{\ddagger}$ = 79.9 and 78.6 kJ/mol for the cross and self-aldol condensations, respectively). In this step the loss of resonance results in a higher transition state energy, and would therefore decrease the reaction rate. Removal of a proton from the α-carbon atom requires the crossing of an additional transition state (TS4) bringing the global free energy barrier to 94 kJ/mol (Table 1), which is slightly lower than for the cross-aldol condensation reaction. This is more or less compensated by the weaker adsorption of the two propanal molecules. Following the free energy profile in Fig. 5, the product yields (cross versus self) are close to each other.

In order to complement and account properly for the topology of the material, periodic density functional theory calculations were also conducted as explained in the computational section. In Fig. 3c the periodic model with encircled active site is displayed. The free energy profiles of the α-methyl-*trans*-cinnamaldehyde formation are shown in Fig. 6. To determine the influence of the framework, we compare cluster and periodic model for the cross-aldol condensation. The theoretical results are given in Table 2, in which the enthalpy and entropy contributions are listed separately. The first adsorption step shows quantitatively large differences: the adsorbed reactants are more strongly bound in the periodic model. For the next steps in the reaction path the free energy differences between the two models remain largely the same. This implies that once the adsorbed complex is formed, confinement effects for the further steps in the reaction route are not differing much, which is not surprising; framework effects only appear again at the end of the reaction path with the desorption of the product (TS6). During the reaction the global free energy profiles, predicted by the two models, are largely similar, apart from a shift of some 20–30 kJ/mol (Fig. 6), but this does not mean that the decomposition into enthalpic and entropic contributions also behaves similarly in the two models. As an illustration, the total free energy barrier of 32.9 kJ/mol predicted by the cluster calculation for step 2 (TS2-c) is close to the value of 35.2 kJ/mol, as resulting from the periodic calculation. However, if we look at the decomposition of the barrier, significant differences in enthalpic and entropic contributions between cluster and periodic models appear: $\Delta H^{\ddagger}$ = 14.3 and 18.6 kJ/mol; $-T\Delta S^{\ddagger}$ = 23.9 and 11.3 kJ/mol, respectively. The same trend is observed in the next steps 4–6. The periodic model predicts a much more stable final product complex, just as was observed for the reactant complex. Obviously, this is a pure confinement effect (State 6-c), and when

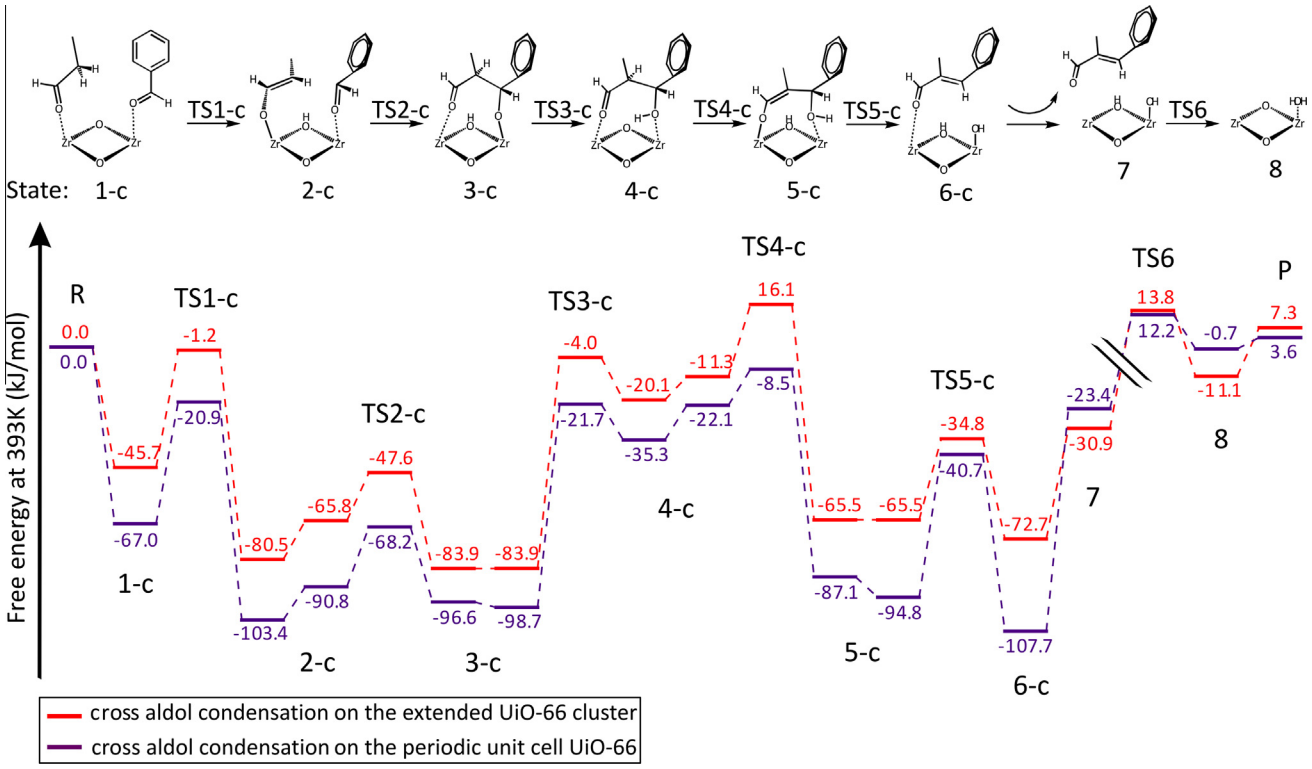

Fig. 6. Schematic representation of the cross-aldol condensation. Comparison of the free energy profiles between two models, cluster (red) and periodic (violet) UiO-66 for the jasminaldehyde formation, calculated at 393 K. Level of theory on the cluster: B3LYP/6-311++G(d,p)-D3//B3LYP/6-31G(d)*. Level of theory on the periodic unit cell: B3LYP-D3(BJ)//PBE-D3(BJ). R corresponds to the reactants in gas phase and the cluster, P corresponds to the final product and water in gas phase and the cluster. Two parallel bars indicate that the main product is no longer present in the catalyst. (For interpretation of the references to color in this figure legend, the reader is referred to the web version of this article.)

Table 2
Enthalpy, entropy and free energy contributions given in kJ/mol for the cross-aldol condensation on the cluster model UiO-66 and UiO-66-NH_2 (B3LYP/6-311++G(d,p)-D3//B3LYP/6-31G(d)*), and on the periodic UiO-66 unit cell (B3LYP-D3(BJ))//PBE-D3(BJ), calculated at 393 K.

		UiO-66						UiO-66-NH_2		
		Cluster model			Periodic model			Cluster model		
		$\Delta H^{\ddagger}$	$-T\Delta S^{\ddagger}$	$\Delta G^{\ddagger}$	$\Delta H^{\ddagger}$	$-T\Delta S^{\ddagger}$	$\Delta G^{\ddagger}$	$\Delta H^{\ddagger}$	$-T\Delta S^{\ddagger}$	$\Delta G^{\ddagger}$
Cross	Step 1	25.8	18.6	44.4	31.1	15.0	46.1	21.0	21.6	42.6
	Step 2	14.3	18.6	32.9	23.9	11.3	35.2	17.2	15.7	32.9
	Step 3	79.9	0.0	79.9	74.5	2.5	77.0	77.0	−0.9	76.1
	Step 4	25.7	10.5	36.2	11.1	15.7	26.8	20.0	13.8	33.8
	Step 5	33.1	−2.4	30.7	56.8	−2.7	54.1	40.1	2.5	42.6
	Steps 3–5	97.0	3.0	100.0	76.9	11.3	88.2	90.7	4.9	95.6

the product is desorbed and removed from the cage, the effect of confinement disappears (State 7).

Summarizing, the periodic model, in which we account for the environment of surrounding linkers and other Zr Lewis acid sites, gives a more accurate description of the system. Nevertheless, the qualitative aspects of the mechanism are fairly well described by the extended cluster model.

The results presented so far show that on UiO-66 the self-condensation reaction is competitive with the cross-aldol condensation reaction and proceeds by the same mechanism. Furthermore the consecutive protonation/deprotonation of the reacting molecules in steps 3–5 was shown to be rate determining.

3.2. Reaction mechanism on UiO-66-NH_2

We first examined the same reaction mechanism for the cross-aldol condensation as found for the pristine UiO-66 with a crucial role for the oxo-atom in the inorganic brick as base site. The free energy profile is shown in Fig. 7 and shows a striking similarity with the profile corresponding to the parent UiO-66. Propanal is activated to the enolate form by proton transfer from the α-carbon to the μ_3-oxygen. The electron-donating amino group on the linker is not actively involved in the reaction and the effects of its presence on the different steps in the reaction profile appear to be minor. However, the amino substitution does lower the adsorption of propanal and benzaldehyde and the activation free energy of the reaction. The total free energy barrier needed to cross the steps 3–5 is somewhat lower (95 kJ/mol) than the 100 kJ/mol for the unfunctionalized UiO-66 (Table 2). Each intermediate state during the condensation reaction on UiO-66-NH_2 is more stabilized with an excess observed in intermediate State 5-c with a free energy of −92.1 kJ/mol, compared with −65.5 kJ/mol in the unsubstituted material. Nevertheless, this remarkable difference has completely disappeared once the final cross-aldol product has been formed even in the adsorbed State 6-c: in both materials the adsorption energy is similar (−72.7 versus −72.4 kJ/mol). Summarizing, the stronger adsorption of the reactants combined with a slightly lower barrier for the amino functionalized material, would point toward a higher catalytic activity.

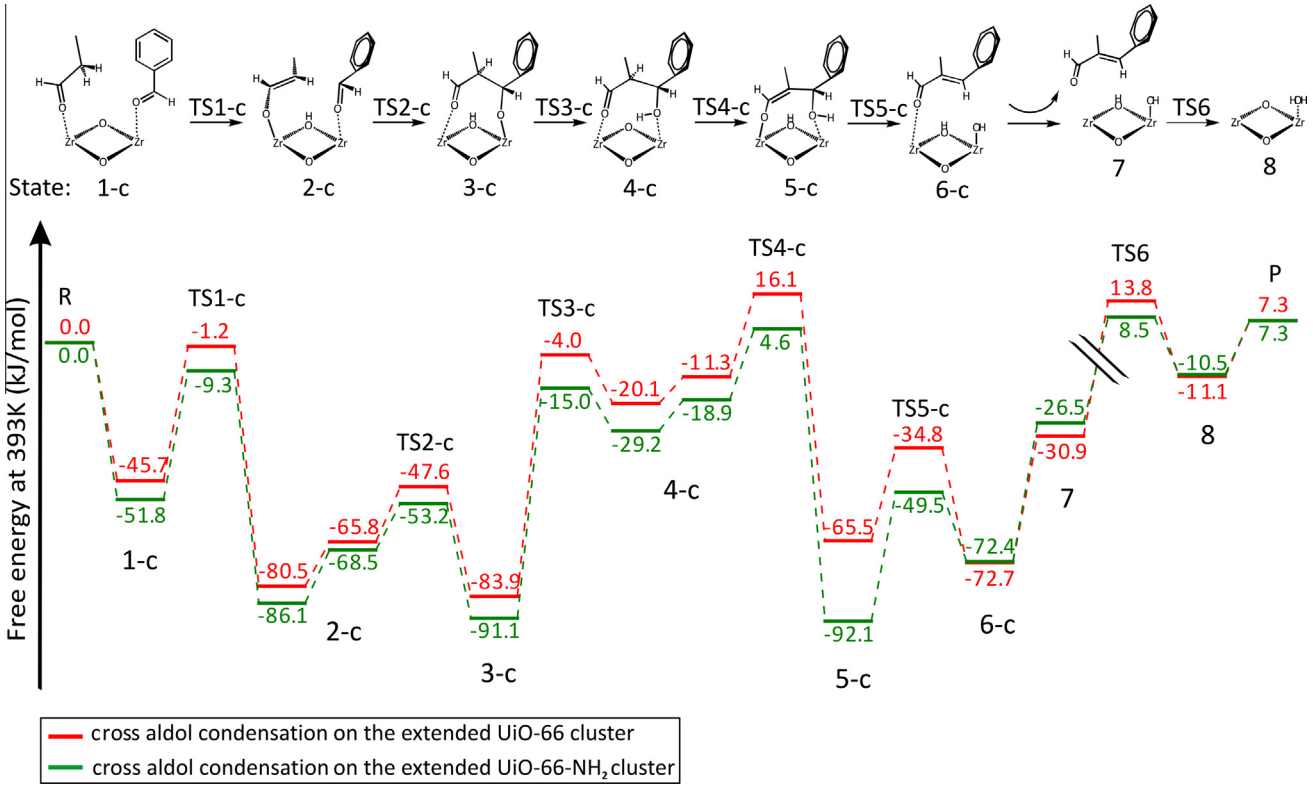

Fig. 7. Comparison of the free energy profiles for the cross-aldol condensation on UiO-66-NH_2 and UiO-66. B3LYP/6-311++G(d,p)-D3//B3LYP/6-31G(d)*, calculated at 393 K. R corresponds to the reactants in gas phase and the cluster, P corresponds to the final product and water in gas phase and the cluster. Two parallel bars indicate that the main product is no longer present in the catalyst.

This is in agreement with recent experimental work [6], as in all papers investigating condensation reactions one stresses the systematic increase of activity when inserting electron-donating amino groups into the linker ligand enlarging the basicity of the UiO-66-NH_2 material. The increase is even larger than we could expect from the free energy profile. It has been believed that the cooperative action between the framework Lewis sites and the amino base groups resulted in high yields for the cross-aldol reaction [6]. It is in line with the conclusion made in a more general experimental study of Vermoortele et al. [23], that the activity of UiO-66 catalysts with coordinatively unsaturated sites can be strongly increased by using functionalized linkers. The superior performance of this acid–base bifunctional catalyst has been confirmed by other experiments. Timofeeva et al. [30] studied the reaction between benzaldehyde and methanol on substituted UiO-66. These authors also confirmed that the increase in Lewis acidity favors the increase of catalytic activity in the acetalization of benzaldehyde with methanol. Some recent experimental work also reports on other pathways directly based on the basicity of the amino group. They mainly consider the Knoevenagel condensation reaction [30,31,39,59–61] but they proposed valuable and constructive routes leading to the formation of the final condensation product with a central role for the amino group. A plausible route has been suggested in the paper of Gascon et al. [59], where clear experimental evidences for the formation of intermediate benzaldimine species in IRMOF-3 and other amino-based MOFs have been given. To support the findings of Gascon et al. [59] a DFT study has been performed on the Knoevenagel condensation of benzaldehyde and ethyl-cyanoacetate taking place in IRMOF-3. This study of Cortese and Duca [62] confirmed the role of imines as important intermediates, but it should be stressed that the catalytic environment of IRMOF-3 is not similar with UiO-66-NH_2 as the former has no other base site than the amino group, while the amino substituted UiO-66 material shows two competitive base sites with the amino group and the oxo-atom near the Lewis acid metal site. A more detailed theoretical investigation is certainly needed to unravel these uncertainties. We therefore examined the pathways as suggested by the abovementioned experimental works, involving Zr Lewis acid sites as well as NH_2 Brønsted base sites:

(i) Firstly, we investigated an earlier proposed mechanism [6] for activation of the methyl group of propanal on the amino function (TSb, Fig. 8). This mechanism implies deprotonation

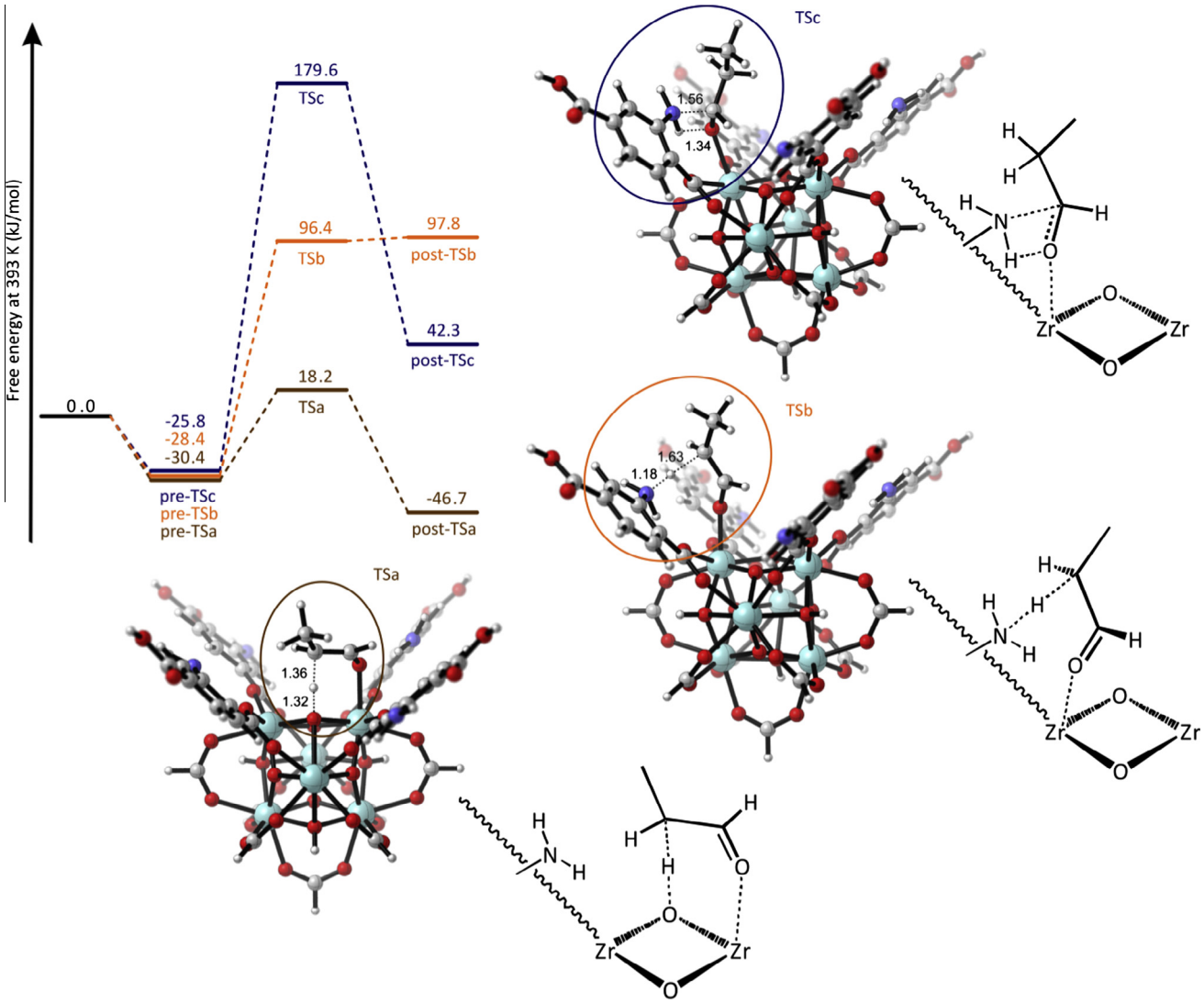

Fig. 8. The free energy barrier of the deprotonation on the oxo-atom (TSa: brown), on the amino group (TSb: orange) and imine formation (TSc: dark blue) on the cluster model. B3LYP/6-311++G(d,p)//B3LYP/6-31G(d)*, calculated at 393 K. Some critical distances are given in Å. The "zig-zag" line in the schematic representation of the TS states corresponds to the terephthalate linker. (For interpretation of the references to color in this figure legend, the reader is referred to the web version of this article.)

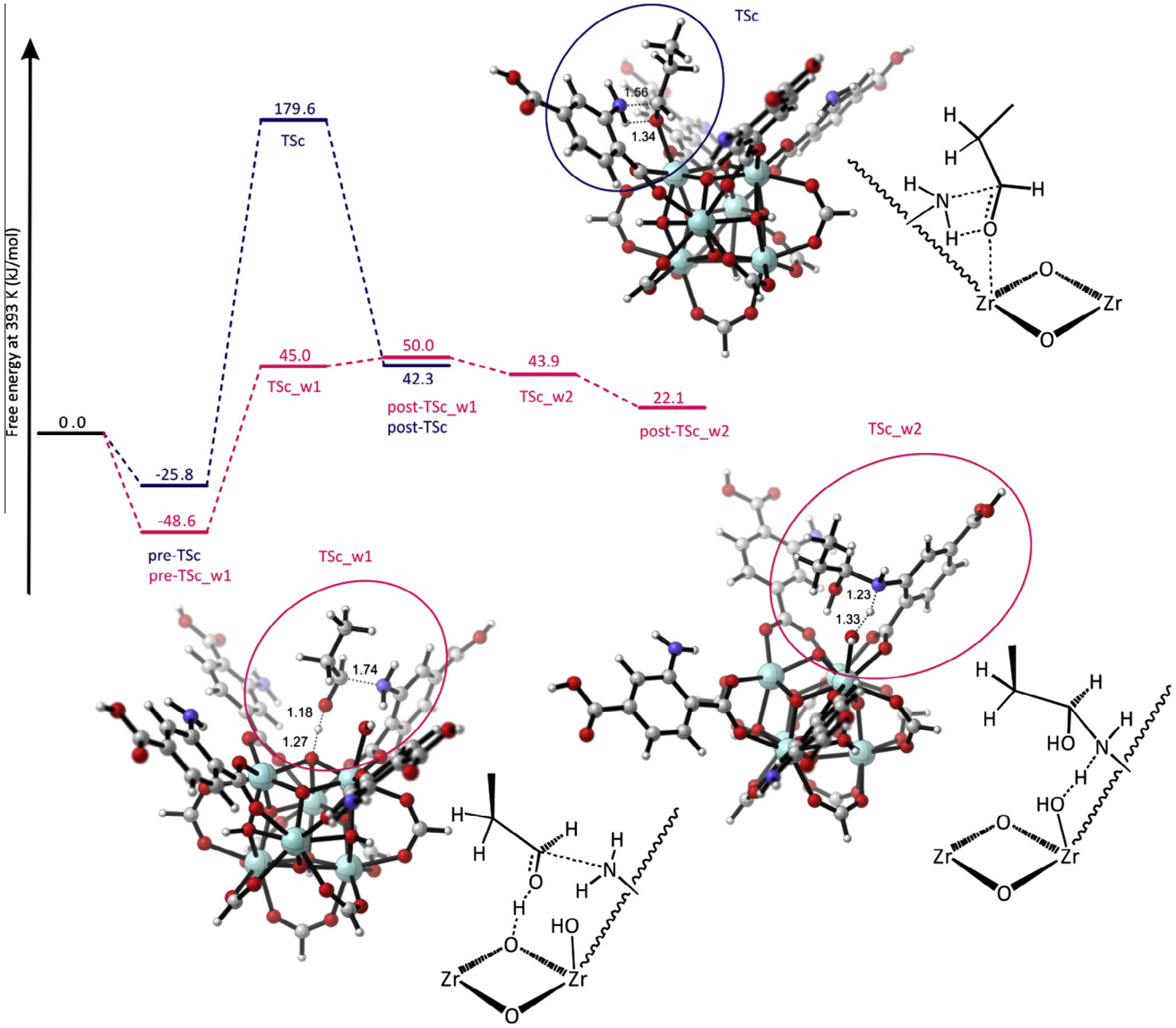

Fig. 9. The free energy barrier of the hemiaminal formation with water as a co-catalyst (TSc_w1 and TSc_w2: pink) and without assisting water molecule (TSc: dark blue) on the cluster model. B3LYP/6-311++G(d,p)//B3LYP/6-31G(d)*, calculated at 393 K. Some critical distances are given in Å. The "zig-zag" line in the schematic representation of the TS states corresponds to the terephthalate linker. (For interpretation of the references to color in this figure legend, the reader is referred to the web version of this article.)

of propanal to form the corresponding carbanion and a protonated amino group. The free energy barrier for proton transfer to the amino group is more than two times higher than for protonation of the oxo-atom ($\Delta G^{\ddagger}$ = 124.8 versus 48.6 kJ/mol). As we can see from Fig. 8, the post-TSb is very unstable and the equilibrium is driven back to the pre-TSb.[1] The theoretical calculations obviously exclude this mechanism, and thus disagree with the suggestion made in Ref. [6], that this pathway could lie at the origin of the increased observed activity for the cross-aldol condensation.

(ii) Secondly, we focused on hemiaminal formation as this is an intermediate step in the formation of a framework-bound imine (Fig. S3), as was already experimentally observed for the Knoevenagel condensation [31,59,61,63]. A pathway was investigated in which 1-propanal is activated on the amino group to form an imine moiety which is preceded by hemiaminal formation (TSc, Fig. 8). However, the free energy barrier between the pre-transition state and the transition state goes up to 205.4 kJ/mol, which is too high to be a plausible reaction route. So, imine formation does not happen via TSc, but if it occurs, the reaction is most probably initiated by a proton shuttle such as water (Fig. S4). To explore such easier reaction routes leading to a bound imine, we elaborate on a reaction mechanism as given in Fig. 9. The reaction induced by water (TSc_w1 and TSc_w2) is a stepwise process. The water molecule is attached to the catalyst by means of two hydroxyl groups: water is heterolytically activated on the material, with a proton on the oxo-atom and a hydroxyl anion on Zr. During the first step (TSc_w1) a hydrogen atom attached to the oxo-atom on the cluster protonates the aldehyde group of propanal. Simultaneously the carbon–nitrogen bond is formed.

The second step of this reaction (TSc_w2) comprises the proton transfer from the amine group to the Zr-bound hydroxyl group.

[1] The free energy of post-TSb structure is higher than the energy of transition state TSb. This is a consequence of thermal corrections. In a profile with electronic energies the TS is higher in energy than the product. E0 (TSb) = −5060.3716 a.u. while E0 (post-TSb) = −5060.3722 a.u. The product state is more bound.

This two-step hemiaminal formation proceeds fast leading to the formation of a relatively stable intermediate. The promoting effect of water during hemiaminal formation is evident. In this case the barrier of about 205 kJ/mol is reduced to 93.6 kJ/mol. This route deserves attention as it leads to imine formation bound to the framework. The imine can further activate benzaldehyde adsorbed on the material, following a catalytic cycle as described by Gascon et al. [59]. The role of propanal and benzaldehyde in pathway TSc can easily be interchanged with the formation of a benzaldimine. The energetics will not alter too much. Anyway this catalytic cycle via imine formation is not excluded when water is present on the catalyst, but is not of such magnitude to disturb the dominant role of pathway TSa, whereby both reactants are adsorbed on adjacent Zr-sites, and propanal is activated via the basic oxo-atom which turns out to be a stronger base than the amino group. The Zr Lewis acid site is clearly favored for propanal activation over the amino Brønsted base site.

From these investigations we exclude other significant catalytic pathways for the UiO-66-NH_2. Our catalytic cycle and the role of amine differ from the previously suggested mechanisms and this behavior has not been observed in experimental studies so far. Beside the enhancement of the catalytic activity resulting from intrinsic electronic effects arising from the amino substituents, it is not excluded that part of the increased activity is due to the presence of a larger amount of defect structures and thus a higher number of catalytic sites within the amino-functionalized material compared to the parent UiO-66 material. But this is a hypothesis as not confirmed by the experiment(s). A similar detailed study, as done in Ref. [23] for the citronellal cyclization, can shed insight in unravelling the effect of substituent groups on the aldol condensation, in a similar fashion as the citronellal cyclization [23]. Such study might serve to design new materials with optimal activity and selectivity, and we would be able to place the catalytic activity of the amino group in relation to other substituent groups.

3.3. Experimental activity of UiO-66 and UiO-66-NH_2

While earlier experimental observations suggested UiO-66-NH_2 to be more selective for the cross-aldol reaction than UiO-66, the computational results indicate that the reaction mechanism on both materials bears many similar traits. In order to confirm this, a new aldol condensation experiment has been performed on the two catalysts but with benzaldehyde and propanal, forming α-methylcinnamaldehyde as main product. The applied experimental methodology is similar as in a previous paper of some of the authors [6], and is given in the experimental methodology section.

The data show that the activity is initially higher for UiO-66-NH_2 than for UiO-66 in otherwise identical conditions (Fig. 10). This higher activity lines up perfectly with the calculated stronger adsorption and slightly lower barriers on the amino-functionalized MOF, as shown in Fig. 7. The fact that especially for the benzaldehyde–propanal pair, the adsorption enthalpy is more negative than for adsorption of two propanal molecules on adjacent open sites can be consistent with the high initial selectivity for cross-aldol reaction on UiO-66-NH_2. The initial activity ratios after 20 min of the reaction indicate that the formation of the cross-aldol condensation product is favored for the amino modified UiO-66-NH_2 (Table 3). However, after 40 min of the reaction we observe an increased production of the cross-aldol product in the pristine UiO-66 compared to the UiO-66-NH_2 (initial activity ratio > 1). The self-aldol condensation product is preferably created on the parent UiO-66 at almost the same quantity during the reaction time of 60 min.

All measurements at different reaction times point toward a selectivity in favor of the cross-aldol product for the two catalysts, which is partly due to the large excess of benzaldehyde used. With

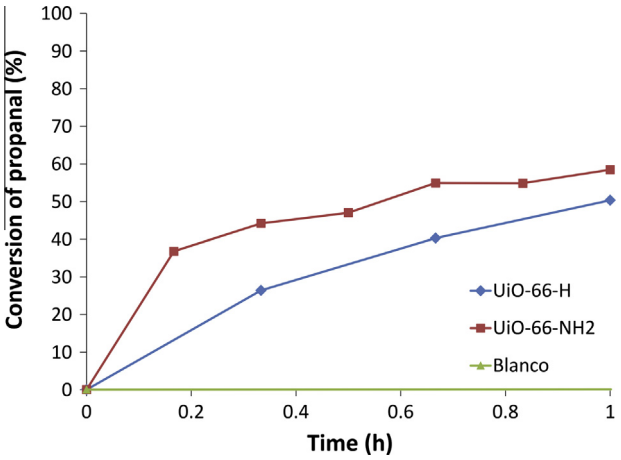

Fig. 10. Time dependence of reaction conversion of propanal on the two catalysts.

Table 3
Activity ratio of UiO-66 versus UiO-66-NH_2 in function of time of cross- and self-aldol product formation for the reaction of benzaldehyde and propanal.

Time (min)	Cross-aldol product	Self-aldol product
20	0.32	1.72
40	1.12	1.88
60	1.77	1.87

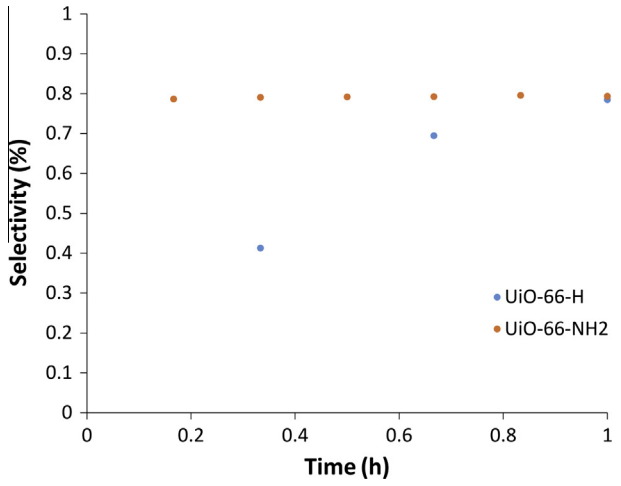

Fig. 11. Selectivity for the formation of the cross-aldol product at the two catalysts.

UiO-66-NH_2, the initial selectivity based on propanal amounts to 79%; this value remains constant during the remainder of the experiment. There is more competition between cross and self-aldol product formation in the parent UiO-66 catalyst, in the initial stage the selectivity toward cross-aldol condensation is only 41%, implying that more propanal is used for self-condensation than for cross-aldol condensation with benzaldehyde (Fig. 11).

Moreover, it is striking that for UiO-66, the selectivity for the cross-aldol product gradually increases as the reaction proceeds. Note that the reaction produces water; as more water is present in the pores, both the adsorption characteristics and the precise nature of the active site, e.g. its hydroxylation degree may change. However, as the trajectories in Figs. 5 and 7 only apply to a pristine, water-free catalyst, the calculations do not allow explaining changes in selectivity during the reaction.

4. Conclusions

In this work, we have studied the mechanism for the cross and self-aldol condensations of propanal and benzaldehyde and the performance of UiO-66 and UiO-66-NH_2 as catalysts. This reaction may be regarded as representative for other cross-aldol condensations, e.g. the condensation of heptanal and benzaldehyde to produce jasminaldehyde. The superior performance of UiO-66-NH_2 was previously suggested to be caused by a bifunctional acid–base character of the material. It has been proposed that the Zr-site in close vicinity of the amino group activates aldehydes to promote the formation of aldimine intermediates from the aldehydes and the amino group. All these experimental findings have not yet been supported by theoretical calculations so far. The current study reveals that the dominant mechanism in the aldol condensation reaction does not differ much for the two catalysts. The rate determining step in the whole process is a proton jump from the catalyst surface (the Zr-oxo cluster) to the carbonyl oxygen of the adsorbed aldol product with free energy barriers of around 100 kJ/mol. This has been confirmed by both free energy calculations on extended clusters and periodic models accounting for the full molecular environment of the catalyst. In view of the experimental hypotheses special attention has been given to bi-functional pathways making use of the amino group as an active basic site. Several alternative pathways have been investigated but they all feature higher activation energies than the standard aldol condensation route with a Zr-Lewis acid site and an oxo-atom basic site. The hydrogen bonding interaction between the amino group and the carboxyl oxygen of the propanal reactant does not show significant catalytic benefits. In this context we demonstrated that imine formation on the UiO-66-NH_2 is possible as soon as water is present on the catalyst. This agrees with conclusions made by Yang *et al.* on the Knoevenagel condensation over UiO-66 catalysts [31].

The new experiments, performed in this work, confirm the higher initial conversion of propanal and the higher initial selectivity for the cross-aldol product in UiO-66-NH_2 compared with the parent UiO-66, but after longer reaction time the experiment rather predicts a nearly similar performance of both catalysts. Our theoretical results indeed predict a slightly higher activity for cross-aldol formation on the amino functionalized material due to a slightly stronger adsorption and slightly lower barriers.

Regarding the production of side-products, we notice that the self-aldol condensation of the aliphatic aldehyde (e.g. propanal or heptanal) is competitive and proceeds simultaneously with the cross-aldol condensation. The experiment clearly reveals a high selectivity in favor of the cross-product in both catalysts but in the parent UiO-66 the competition with the self-aldol condensation is high in the very early stages of the reaction. Selectivities are dynamic features which are not reproducible from free energy profiles, obtained with static theoretical calculations. The availability of active metal sites in function of reaction time may also affect the change of activity ratio of UiO-66 versus UiO-66-NH_2 but requires more advanced techniques. This study might serve to design new materials with optimal activity and selectivity.

Acknowledgments

J.H., B.B., V.V.S. and D.D.V. acknowledge funding from the Scientific Research-Foundation Flanders (FWO) (project number 3G048612). M.V. acknowledges the FWO for a postdoctoral fellowship. V.V.S., D.D.V. and M.W. acknowledge BELSPO in the frame of IAP-PAI P7/05. V.V.S. acknowledges funding from the European Research Council under the European Community's Seventh Framework Programme [FP7(2007–2013) ERC grant agreement number 240483] and from the European Union Horizon 2020 research and innovation programme (consolidation ERC grant, agreement No. 647755-DYNPOR (2015–2020)). The computational resources and services used in this work were provided by VSC (Flemish Supercomputer Center), funded by the Hercules foundation and the Flemish Government – department EWI.

Appendix A. Supplementary material

Supplementary data associated with this article can be found, in the online version, at http://dx.doi.org/10.1016/j.jcat.2015.08.015.

References

[1] M.J. Climent, A. Corma, V. Fornes, R. Guil-Lopez, S. Iborra, Aldol condensations on solid catalysts: a cooperative effect between weak acid and base sites, Adv. Synth. Catal. 344 (2002) 1090–1096.
[2] M.J. Climent, A. Corma, R. Guil-Lopez, S. Iborra, J. Primo, Use of mesoporous MCM-41 aluminosilicates as catalysts in the preparation of fine chemicals – a new route for the preparation of Jasminaldehyde with high selectivity, J. Catal. 175 (1998) 70–79.
[3] S.K. Sharma, P.A. Parikh, R.V. Jasra, Eco-friendly synthesis of jasminaldehyde by condensation of 1-heptanal with benzaldehyde using hydrotalcite as a solid base catalyst, J. Mol. Catal. A – Chem. 286 (2008) 55–62.
[4] M.J. Climent, A. Corma, H. Garcia, R. Guil-Lopez, S. Iborra, V. Fornes, Acid–base bifunctional catalysts for the preparation of fine chemicals: synthesis of jasminaldehyde, J. Catal. 197 (2001) 385–393.
[5] S.K. Sharma, H.A. Patel, R.V. Jasra, Synthesis of jasminaldehyde using magnesium organo silicate as a solid base catalyst, J. Mol. Catal. A – Chem. 280 (2008) 61–67.
[6] F. Vermoortele, R. Ameloot, A. Vimont, C. Serre, D. De Vos, An amino-modified Zr-terephthalate metal–organic framework as an acid–base catalyst for cross-aldol condensation, Chem. Commun. 47 (2011) 1521–1523.
[7] G. Ferey, Hybrid porous solids: past, present, future, Chem. Soc. Rev. 37 (2008) 191–214.
[8] J.L.C. Rowsell, O.M. Yaghi, Metal–organic frameworks: a new class of porous materials, Micropor. Mesopor. Mater. 73 (2004) 3–14.
[9] O.M. Yaghi, M. O'Keeffe, N.W. Ockwig, H.K. Chae, M. Eddaoudi, J. Kim, Reticular synthesis and the design of new materials, Nature 423 (2003) 705–714.
[10] B. Van de Voorde, B. Bueken, J. Denayer, D. De Vos, Adsorptive separation on metal–organic frameworks in the liquid phase, Chem. Soc. Rev. 43 (2014) 5766–5788.
[11] M. Kim, S.M. Cohen, Discovery, development, and functionalization of Zr(IV)-based metal–organic frameworks, CrystEngComm 14 (2012) 4096–4104.
[12] P. Valvekens, F. Vermoortele, D. De Vos, Metal–organic frameworks as catalysts: the role of metal active sites, Catal. Sci. Technol. 3 (2013) 1435–1445.
[13] D. Farrusseng, S. Aguado, C. Pinel, Metal–organic frameworks: opportunities for catalysis, Angew. Chem. Int. Ed. 48 (2009) 7502–7513.
[14] J. Lee, O.K. Farha, J. Roberts, K.A. Scheidt, S.T. Nguyen, J.T. Hupp, Metal–organic framework materials as catalysts, Chem. Soc. Rev. 38 (2009) 1450–1459.
[15] A. Dhakshinamoorthy, M. Alvaro, H. Garcia, Metal–organic frameworks as heterogeneous catalysts for oxidation reactions, Catal. Sci. Technol. 1 (2011) 856–867.
[16] L.Q. Ma, C. Abney, W.B. Lin, Enantioselective catalysis with homochiral metal–organic frameworks, Chem. Soc. Rev. 38 (2009) 1248–1256.
[17] A. Dhakshinamoorthy, M. Alvaro, H. Garcia, Commercial metal–organic frameworks as heterogeneous catalysts, Chem. Commun. 48 (2012) 11275–11288.
[18] A. Corma, H. Garcia, F.X.L.I. Xamena, Engineering metal organic frameworks for heterogeneous catalysis, Chem. Rev. 110 (2010) 4606–4655.
[19] J.H. Cavka, S. Jakobsen, U. Olsbye, N. Guillou, C. Lamberti, S. Bordiga, K.P. Lillerud, A new zirconium inorganic building brick forming metal organic frameworks with exceptional stability, J. Am. Chem. Soc. 130 (2008) 13850–13851.
[20] V. Guillerm, S. Gross, C. Serre, T. Devic, M. Bauer, G. Ferey, A zirconium methacrylate oxocluster as precursor for the low-temperature synthesis of porous zirconium(IV) dicarboxylates, Chem. Commun. 46 (2010) 767–769.
[21] M. Kandiah, M.H. Nilsen, S. Usseglio, S. Jakobsen, U. Olsbye, M. Tilset, C. Larabi, E.A. Quadrelli, F. Bonino, K.P. Lillerud, Synthesis and stability of tagged UiO-66 Zr-MOFs, Chem. Mater. 22 (2010) 6632–6640.
[22] L. Valenzano, B. Civalleri, S. Chavan, S. Bordiga, M.H. Nilsen, S. Jakobsen, K.P. Lillerud, C. Lamberti, Disclosing the complex structure of UiO-66 metal organic framework: a synergic combination of experiment and theory, Chem. Mater. 23 (2011) 1700–1718.
[23] F. Vermoortele, M. Vandichel, B. Van de Voorde, R. Ameloot, M. Waroquier, V. Van Speybroeck, D.E. De Vos, Electronic effects of linker substitution on lewis acid catalysis with metal–organic frameworks, Angew. Chem. Int. Ed. 51 (2012) 4887–4890.
[24] M. Vandichel, J. Hajek, F. Vermoortele, D.E. De Vos, M. Waroquier, V. Van Speybroeck, Active site engineering of UiO-66 type metal–organic frameworks

by intentional creation of defects: a theoretical rationalization, CrystEngComm 17 (2015) 395–406.
[25] Q.Y. Yang, A.D. Wiersum, P.L. Llewellyn, V. Guillerm, C. Serred, G. Maurin, Functionalizing porous zirconium terephthalate UiO-66(Zr) for natural gas upgrading: a computational exploration, Chem. Commun. 47 (2011) 9603–9605.
[26] M. Kandiah, S. Usseglio, S. Svelle, U. Olsbye, K.P. Lillerud, M. Tilset, Post-synthetic modification of the metal–organic framework compound UiO-66, J. Mater. Chem. 20 (2010) 9848–9851.
[27] G.E. Cmarik, M. Kim, S.M. Cohen, K.S. Walton, Tuning the adsorption properties of UiO-66 via ligand functionalization, Langmuir 28 (2012) 15606–15613.
[28] S.M. Chavan, G.C. Shearer, S. Svelle, U. Olsbye, F. Bonino, J. Ethiraj, K.P. Lillerud, S. Bordiga, Synthesis and characterization of amine-functionalized mixed-ligand metal–organic frameworks of UiO-66 topology, Inorg. Chem. 53 (2014) 9509–9515.
[29] T. Lescouet, C. Chizallet, D. Farrusseng, The origin of the activity of amine-functionalized metal-organic frameworks in the catalytic synthesis of cyclic carbonates from epoxide and CO_2, ChemCatChem 4 (2012) 1725–1728.
[30] M.N. Timofeeva, V.N. Panchenko, J.W. Jun, Z. Hasan, M.M. Matrosova, S.H. Jhung, Effects of linker substitution on catalytic properties of porous zirconium terephthalate UiO-66 in acetalization of benzaldehyde with methanol, Appl. Catal. A – Gen. 471 (2014) 91–97.
[31] Y. Yang, H.F. Yao, F.G. Xi, E.Q. Gao, Amino-functionalized Zr(IV) metal–organic framework as bifunctional acid–base catalyst for Knoevenagel condensation, J. Mol. Catal. A – Chem. 390 (2014) 198–205.
[32] R. Kardanpour, S. Tangestaninejad, V. Mirkhani, M. Moghadam, I. Mohammadpoor-Baltork, A.R. Khosropour, F. Zadehahmadi, Highly dispersed palladium nanoparticles supported on amino functionalized metal–organic frameworks as an efficient and reusable catalyst for Suzuki cross-coupling reaction, J. Organomet. Chem. 761 (2014) 127–133.
[33] J. Zhu, P.C. Wang, M. Lu, Selective oxidation of benzyl alcohol under solvent-free condition with gold nanoparticles encapsulated in metal–organic framework, Appl. Catal. A – Gen. 477 (2014) 125–131.
[34] Y.M. Chung, H.Y. Kim, W.S. Ahn, Friedel–Crafts acylation of p-xylene over sulfonated zirconium terephthalates, Catal. Lett. 144 (2014) 817–824.
[35] Z.Y. Guo, C.X. Xiao, R.V. Maligal-Ganesh, L. Zhou, T.W. Goh, X.L. Li, D. Tesfagaber, A. Thiel, W.Y. Huang, Pt nanoclusters confined within metal organic framework cavities for chemoselective cinnamaldehyde hydrogenation, ACS Catal. 4 (2014) 1340–1348.
[36] K. Leus, M. Vandichel, Y.Y. Liu, I. Muylaert, J. Musschoot, S. Pyl, H. Vrielinck, F. Callens, G.B. Marin, C. Detavernier, P.V. Wiper, Y.Z. Khimyak, M. Waroquier, V. Van Speybroeck, P. Van der Voort, The coordinatively saturated vanadium MIL-47 as a low leaching heterogeneous catalyst in the oxidation of cyclohexene, J. Catal. 285 (2012) 196–207.
[37] M. Vandichel, F. Vermoortele, S. Cottenie, D.E. De Vos, M. Waroquier, V. Van Speybroeck, Insight in the activity and diastereoselectivity of various Lewis acid catalysts for the citronellal cyclization, J. Catal. 305 (2013) 118–129.
[38] T. Verstraelen, V. Van Speybroeck, M. Waroquier, ZEOBUILDER: a GUI toolkit for the construction of complex molecular structures on the nanoscale with building blocks, J. Chem. Inf. Model. 48 (2008) 1530–1541.
[39] M. Vandichel, S. Biswas, K. Leus, J. Paier, J. Sauer, T. Verstraelen, P. Van Der Voort, M. Waroquier, V. Van Speybroeck, Catalytic performance of vanadium MIL-47 and linker-substituted variants in the oxidation of cyclohexene: a combined theoretical and experimental approach, ChemPlusChem 79 (2014) 1183–1197.
[40] M.J. Frisch, G.W. Trucks, H.B. Schlegel, G.E. Scuseria, M.A. Robb, J.R. Cheeseman, G. Scalmani, V. Barone, B. Mennucci, G.A. Petersson, H. Nakatsuji, M. Caricato, X. Li, H.P. Hratchian, A.F. Izmaylov, J. Bloino, G. Zheng, J.L. Sonnenberg, M. Hada, M. Ehara, K. Toyota, R. Fukuda, J. Hasegawa, M. Ishida, T. Nakajima, Y. Honda, O. Kitao, H. Nakai, T. Vreven, J.A. Montgomery Jr., J.E. Peralta, F. Ogliaro, M. Bearpark, J.J. Heyd, E. Brothers, K.N. Kudin, V.N. Staroverov, R. Kobayashi, J. Normand, K. Raghavachari, A. Rendell, J.C. Burant, S.S. Iyengar, J. Tomasi, M. Cossi, N. Rega, N.J. Millam, M. Klene, J.E. Knox, J.B. Cross, V. Bakken, C. Adamo, J. Jaramillo, R. Gomperts, R.E. Stratmann, O. Yazyev, A.J. Austin, R. Cammi, C. Pomelli, J.W. Ochterski, R.L. Martin, K. Morokuma, V.G. Zakrzewski, G.A. Voth, P. Salvador, J.J. Dannenberg, S. Dapprich, A.D. Daniels, O. Farkas, J.B. Foresman, J.V. Ortiz, J. Cioslowski, D.J. Fox, Gaussian 09, Revision D.01, Gaussian Inc., Wallingford, CT, 2009.
[41] P.J. Hay, W.R. Wadt, Abinitio effective core potentials for molecular calculations – potentials for the transition-metal atoms Sc to Hg, J. Chem. Phys. 82 (1985) 270–283.
[42] P.J. Hay, W.R. Wadt, Abinitio effective core potentials for molecular calculations – potentials for K to Au including the outermost core orbitals, J. Chem. Phys. 82 (1985) 299–310.
[43] W.R. Wadt, P.J. Hay, Abinitio effective core potentials for molecular calculations – potentials for main group elements Na to Bi, J. Chem. Phys. 82 (1985) 284–298.
[44] S. Grimme, J. Antony, S. Ehrlich, H. Krieg, A consistent and accurate ab initio parametrization of density functional dispersion correction (DFT-D) for the 94 elements H–Pu, J. Chem. Phys. 132 (2010).
[45] G. Kresse, J. Hafner, Abinitio molecular-dynamics for liquid-metals, Phys. Rev. B 47 (1993) 558–561.
[46] G. Kresse, J. Hafner, Ab-initio molecular-dynamics simulation of the liquid-metal amorphous–semiconductor transition in germanium, Phys. Rev. B 49 (1994) 14251–14269.
[47] G. Kresse, J. Furthmuller, Efficiency of ab-initio total energy calculations for metals and semiconductors using a plane-wave basis set, Comput. Mater. Sci. 6 (1996) 15–50.
[48] G. Kresse, J. Furthmuller, Efficient iterative schemes for ab initio total-energy calculations using a plane-wave basis set, Phys. Rev. B 54 (1996) 11169–11186.
[49] S. Grimme, S. Ehrlich, L. Goerigk, Effect of the damping function in dispersion corrected density functional theory, J. Comput. Chem. 32 (2011) 1456–1465.
[50] G. Kresse, D. Joubert, From ultrasoft pseudopotentials to the projector augmented-wave method, Phys. Rev. B 59 (1999) 1758–1775.
[51] P.E. Blochl, Projector augmented-wave method, Phys. Rev. B 50 (1994) 17953–17979.
[52] V. Van Speybroeck, K. De Wispelaere, J. Van der Mynsbrugge, M. Vandichel, K. Hemelsoet, M. Waroquier, First principle chemical kinetics in zeolites: the methanol-to-olefin process as a case study, Chem. Soc. Rev. 43 (2014) 7326–7357.
[53] B.A. De Moor, A. Ghysels, M.F. Reyniers, V. Van Speybroeck, M. Waroquier, G.B. Marin, Normal mode analysis in zeolites: toward an efficient calculation of adsorption entropies, J. Chem. Theory Comput. 7 (2011) 1090–1101.
[54] A. Ghysels, D. Van Neck, M. Waroquier, Cartesian formulation of the mobile block Hessian approach to vibrational analysis in partially optimized systems, J. Chem. Phys. 127 (2007).
[55] M.T. Reetz, A. Meiswinkel, G. Mehler, K. Angermund, M. Graf, W. Thiel, R. Mynott, D.G. Blackmond, Why are BINOL-based monophosphites such efficient ligands in Rh-catalyzed asymmetric olefin hydrogenation?, J Am. Chem. Soc. 127 (2005) 10305–10313.
[56] P.J. Donoghue, P. Helquist, P.O. Norrby, O. Wiest, Development of a Q2MM force field for the asymmetric rhodium catalyzed hydrogenation of enamides, J. Chem. Theory Comput. 4 (2008) 1313–1323.
[57] A. Ghysels, T. Verstraelen, K. Hemelsoet, M. Waroquier, V. Van Speybroeck, TAMkin: a versatile package for vibrational analysis and chemical kinetics, J. Chem. Inf. Model. 50 (2010) 1736–1750.
[58] F. Vermoortele, B. Bueken, G. Le Bars, B. Van de Voorde, M. Vandichel, K. Houthoofd, A. Vimont, M. Daturi, M. Waroquier, V. Van Speybroeck, C. Kirschhock, D.E. De Vos, Synthesis modulation as a tool to increase the catalytic activity of metal–organic frameworks: the unique case of UiO-66(Zr), J. Am. Chem. Soc. 135 (2013) 11465–11468.
[59] J. Gascon, U. Aktay, M.D. Hernandez-Alonso, G.P.M. van Klink, F. Kapteijn, Amino-based metal–organic frameworks as stable, highly active basic catalysts, J. Catal. 261 (2009) 75–87.
[60] J.D. Bass, A. Solovyov, A.J. Pascall, A. Katz, Acid–base bifunctional and dielectric outer-sphere effects in heterogeneous catalysis: a comparative investigation of model primary amine catalysts, J. Am. Chem. Soc. 128 (2006) 3737–3747.
[61] M. Hartmann, M. Fischer, Amino-functionalized basic catalysts with MIL-101 structure, Micropor. Mesopor. Mater. 164 (2012) 38–43.
[62] R. Cortese, D. Duca, A DFT study of IRMOF-3 catalysed Knoevenagel condensation, Phys. Chem. Chem. Phys. 13 (2011) 15995–16004.
[63] V.N. Panchenko, M.M. Matrosova, J. Jeon, J.W. Jun, M.N. Timofeeva, S.H. Jhung, Catalytic behavior of metal–organic frameworks in the Knoevenagel condensation reaction, J. Catal. 316 (2014) 251–259.